Scripta Materialia 150 (2018) 139–142

Contents lists available at ScienceDirect

Scripta Materialia

journal homepage: www.elsevier.com/locate/scriptamat

Regular article

Understanding slow-growing alumina scale mediated by reactive elements: Perspective via local metal-oxygen bonding strength

Shun-Li Shang [a,*], Yi Wang [a], Brian Gleeson [b], Zi-Kui Liu [a]

[a] Department of Materials Science and Engineering, The Pennsylvania State University, University Park, PA 16802, United States
[b] Department of Mechanical Engineering and Materials Science, University of Pittsburgh, Pittsburgh, PA 15261, United States

ARTICLE INFO

Article history:
Received 11 February 2018
Received in revised form 28 February 2018
Accepted 1 March 2018
Available online xxxx

Keywords:
Alumina scale
Reactive elements
Oxides
Phonon
First principles calculations

ABSTRACT

Interatomic bonding strength/energy can be quantified by stretching force constants (SFC) after first-principles phonon calculations. Here, we show that the slow-growing alumina (α-Al_2O_3) scale mediated by reactive elements (REs) can be understood via the strong RE—O bonding energy from the present SFC model applied to oxides (Al_2O_3, Cr_2O_3, Ti_2O_3, ZrO_2, HfO_2, Y_2O_3, and La_2O_3), Al_3M, and $Al_{47}MO_{72}$ (M = Cr, Ti, Zr, Hf, Y, and La). The present model indicates that Hf is the best RE in retarding alumina scale growth, agreeing with the analyses from bulk modulus, melting point, and enthalpy of formation of oxides, and experimental observations.

A dense, continuous, slow-growing, relatively chemically inert and adherent oxide scale is essential for protecting an underlying alloy from oxidation and hot corrosion [1,2]. For example, the thermally grown oxide (TGO) layer within the thermal barrier coating (TBC) system, commonly alumina (α-Al_2O_3), forms in the high-temperature environments of aircraft and industrial gas-turbine engines [3,4]. The Al_2O_3 scale is believed to grow predominantly by oxygen (O) inward diffusion, combined with non-trivial aluminum (Al) outward diffusion, on alumina grain-boundaries [1,5]. Adding reactive elements (REs) such as the present focus of Ti, Zr, Hf, Y, and La, has been found to significantly reduce the growth rate of Al_2O_3 scale [1,5–7]. In particular, Hf shows exceptional effectiveness in comparison with such as Y and Zr [8,9].

The reason why REs are so effective in improving scale performance is still unclear [7], albeit numerous mechanisms have been proposed. Cho et al. [10] suggested a "site-blocking" effect on diffusion by oversized segregant cations within the TGO grain-boundaries, but this hypothesis fails to explain the fact that the smaller size Hf has a more beneficial effect than the larger size Y and Zr [8]. Heuer et al. [5,11] proposed that the segregation of REs on alumina grain-boundaries could reduce Al ionization by modifying the grain-boundary donor and acceptor states, rather than any blocking of diffusion pathways. They suggested that the grain-boundary diffusion occurs via charged jogs instead of the jumping of isolated point defects in the high-angle grain-boundaries, indicating the connection of production/annihilation of the charged Al and O vacancies, and in turn, their diffusivities on grain-boundaries. In a different paper, the present authors [8] recently showed that the metal-oxygen (M—O) bonding strength can be used to understand the effectiveness of REs in retarding the rate of alumina-scale growth. This understanding considers that the diffusion of oxygen involves the breaking of M—O bonds and that the diffusion of aluminum, in turn, relies on oxygen diffusion due to charge-compensation reactions [5,11].

Qualitative M—O bonding strength can be estimated by global properties of oxides due to the dominated M—O bonding in oxides, for example, bulk modulus, melting point, and enthalpy of formation [8]. Due to the local nature of interatomic bonding, quantitative bonding strength between two atoms of interest can be evaluated by force constants, i.e., the Hessian matrix of second derivatives of energy with respect to displacement. Force constants allow quantitative analyses of the extent of interaction or bonding between atomic pairs [12,13]. A large and positive force constant suggests strong interaction (bonding), while a negative force constant indicates that the atomic pairs tend to separate from each other. A zero force constant implies that the two atoms do not interact under the given atomic environments. We believe that force constants are more suitable to characterize bonding strength between atomic pairs in comparison with such as electronegativity which describe the tendency of an atom to attract electrons towards itself.

Force constants between every two atoms (separated by vector $\mathbf{u}$) can be represented by a 3×3 matrix (denoted by $\mathbf{F}$) with nine components. It is more convenient to quantify interatomic bonding using only the bending force constant (BFC) and especially the major contribution

* Corresponding author.
E-mail address: sus26@psu.edu (S.-L. Shang).

https://doi.org/10.1016/j.scriptamat.2018.03.002
1359-6462/

of the stretching force constant (SFC or f_s for short) [12,13]. Both BFC and SFC can be calculated using the projections of force constants **F** perpendicular and parallel to **u**, respectively. For instance,

$$f_s = \hat{\mathbf{u}} \cdot \mathbf{F} \cdot \hat{\mathbf{u}}^T \quad (1)$$

where $\hat{\mathbf{u}}$ is a 1×3 unit vector of **u** and the superscript T indicates transposition. SFC and the associated bond length between every two atoms can be used to probe the origin of alumina-scale growth affected by the reactive elements such as the present focus: Ti, Zr, Hf, Y and La. In addition, alloying constituent Cr is also studied herein since it is another key element to form a protective α-Cr_2O_3 scale, which is isostructural with α-Al_2O_3 (i.e., corundum, hexagonal close-packed).

Metal-oxygen (M—O) and metal-aluminum (M—Al) force constants in the present work are calculated based on the stable oxides (α-Al_2O_3, α-Cr_2O_3, Ti_2O_3, ZrO_2, HfO_2, Y_2O_3, and La_2O_3), dilute M in alumina (i.e., $Al_{47}MO_{72}$, see Supplementary Fig. S1), and Al_3M compounds (Al_3Cr, Al_3Ti, Al_3Zr, Al_3Hf, Al_3Y, and Al_3La); see Supplementary Table S1 for details. It is noted that force constants as a function of bond length are usually transferable across different and especially similar atomic environments [14], making the present analysis reasonable.

All force constants in the present work are calculated using the Vienna Ab initio Simulation Package (VASP) [15]. The ion-electron interaction is described by the projector augmented wave (PAW) method [16]. The exchange-correlation (X-C) energy functional is mainly described by the improved generalized gradient approximation for densely packed solids and their surfaces, i.e., PBEsol [17]. During VASP calculations, the plane wave cutoff energies are set at 500 eV for oxides (including $Al_{47}MO_{72}$) and 350 eV for Al_3M, and the spin polarization is included for all Cr-containing calculations. The selected valence-electron configurations for each element are the same as those used by Materials Project [18,19]. More details of first-principles calculations are given in Supplementary Table S1, including structural details, supercell sizes, and *k*-point meshes for sampling the Brillouin zone for each oxide, $Al_{47}MO_{72}$, or Al_3M. The Supplementary Material also shows additional results from first-principles calculations, including (i) equilibrium properties (volume V_0, bulk modulus B_0, and its pressure derivative B') fitted by a four-parameter Birch-Murnaghan equation of state (EOS) [20], see Supplementary Table S1; (ii) a comparison of the calculated and experimental V_0 and B_0 for oxides, see Supplementary Fig. S2; and (iii) phonon densities of states for oxides and Al_3M predicted by the YPHON code [21], see Supplementary Fig. S3. These properties are not the present focus but can be used to judge the quality of the present first-principles calculations.

Fig. 1a shows the calculated SFCs at 0 K for various metal-oxygen (M—O) pairs based on the stable oxides and the dilute alloying elements M in α-Al_2O_3 (i.e., $Al_{47}MO_{72}$). Note that the key SFC is the largest SFC (denoted by f_{s0}) with usually the shortest bond length r_0, for example, $f_{s0} = 5.62$ eV/Å^2 with $r_0 = 1.86$ Å for the Al—O bond in bulk Al_2O_3 (see the black and filled triangle on the left side of Fig. 1a). It can be seen that all the r_0 values of RE—O (RE = Ti, Zr, Hf, Y, and La) and Cr—O are longer than those of Al—O based on the oxides and $Al_{47}MO_{72}$ (i.e., $r_0 =$ 1.95–2.35 Å versus $r_0 =$ 1.80–1.86 Å). However, the largest SFC (i.e., f_{s0} with length r_0) of each RE—O or Cr—O in oxide case (see the filled symbols) is comparable with and even higher than the f_{s0} of Al—O, with the largest f_{s0} value being for the Hf—O bond followed by those of Cr—O and Zr—O. When REs or Cr dissolve in α-Al_2O_3, the largest SFCs with the shortest M—O bonds (viz., f_{s0} with length r_0) increase dramatically due mainly to the decrease of M—O bond lengths in α-Al_2O_3, especially for the Y—O and La—O bonds with $f_{s0} =$ 3–4 eV/Å^2 increased to 13–14 eV/Å^2; see the symbols connected by the dotted lines in Fig. 1a. In addition, the increased f_{s0} values of M—O bonds in $Al_{47}MO_{72}$ (here, M ≠ Al) are more significant than the corresponding increase of f_{s0} of Al—O; see the open symbols connected by the dot-dashed lines in Fig. 1a. It should be noted that Cr may be expected to dissolve in Al_2O_3 instead of segregated to grain-boundaries [1]. However, the solubility

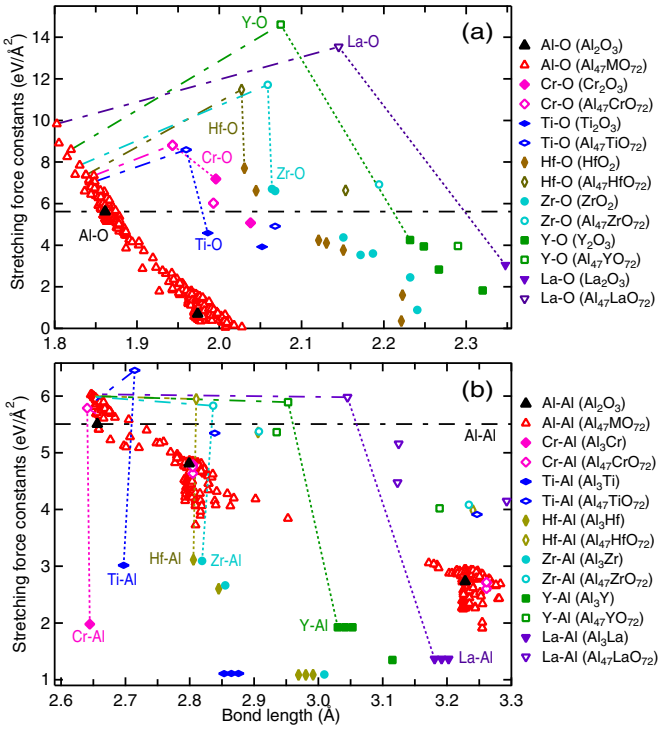

Fig. 1. Calculated stretching force constants (SFCs) at 0 K by PBEsol between the metal-oxygen (M—O) (a) and metal-aluminum (M—Al) (b) atoms based on oxides, Al_3M, and the dilute M-containing α-Al_2O_3 ($Al_{47}MO_{72}$). The dot lines connect the maximal M—O (or M—Al) SFCs in oxides (or Al_3M) and $Al_{47}MO_{72}$. The dot-dashed lines connect the maximal M—O (or M—Al) and Al—O (or Al—Al) SFCs in $Al_{47}MO_{72}$.

of REs in Al_2O_3 is very low, for example, the HfO_2 doping level was found to be 100–200 ppm in Al_2O_3 at 1400 °C [22]. In the real system, the REs are mainly segregated on the Al_2O_3 grain boundaries [1,5], where diffusion would mostly take place. In these lower-symmetry environments, the RE—O (here, RE ≠ Cr) bonds can probably relax close to their equilibrium lengths as shown in the RE-containing concentrated oxides. Correspondingly, the SFCs of these RE—O bond lengths are expected to be similar to those in the RE-containing concentrated oxides, but these SFCs may change up to the cases in $Al_{47}MO_{72}$ when REs dissolve in Al_2O_3, see Fig. 1a.

The variations of bond lengths and SFCs of M—Al in Al_3M and $Al_{47}MO_{72}$ are similar to the M—O case in Fig. 1a; see Fig. 1b. However, the Al-M SFCs (here, M ≠ Al) in Fig. 1b are much lower than the Al—Al SFCs in α-Al_2O_3, for example, $f_{s0} =$ 2–3 eV/Å^2 for Al—M versus $f_{s0} =$ 5.5 eV/Å^2 for Al—Al; see the symbols connected by the dotted lines in Fig. 1b. The M—Al bonding strengths in Fig. 1b are hence ignored during the analyses of alumina scale growth. Force constants in Fig. 1 suggest that the REs influence the diffusion of oxygen due to the strong RE—O bonding, and in turn, the diffusion of aluminum, on the grain-boundaries of alumina via a mechanism such as the charge compensation reactions to generated the Al/O charged vacancies proposed by Heuer et al. [5,11].

The growth of alumina scale relates to the diffusion of oxygen through the breaking of M—O bonds by exceeding the diffusion activation energy *Q* of oxygen. The *Q* values can be estimated via the global properties of oxides [8,23], since the properties of oxides are mainly controlled by the M—O bonds (see such as Supplementary Fig. S4):

$$Q \propto B_0 V_0 \propto RT_m \propto -\Delta H_{298} \quad (2)$$

where the bulk modulus B_0 and volume V_0 for the oxides of interest are shown in Supplementary Table S1, *R* is the gas constant, T_m the melting point, and ΔH_{298} the enthalpy of formation at 298 K. The introduction of Eq. (2) considers the facts that (i) the M—O bonds with shorter bond

lengths are stronger than the O—O bonds with longer bond lengths, see such as Supplementary Fig. S4 for the cases of Al_2O_3 and HfO_2; (ii) the bond stretching can be characterized by bulk modulus, and the work done in stretching bond to failure is proportional to B_0V_0 [23,24]; and (iii) heat can break bonds, causing melting (or sublimation), and the thermal energy at the melting point is RT_m for each principal vibrational mode [24]. Similar to Eq. (2), we propose that the diffusion activation energy Q used to break the M—O bonds can be characterized by the largest SFC, f_{s0} (its unit is energy per unit area such as eV/Å^2; see Fig. 1), and the associated bond length r_0,

$$Q \propto f_{s0} r_0^2 \tag{3}$$

Fig. 2a shows the variations of B_0V_0 of oxides and $f_{s0}r_0^2$ of M—O bonds in oxides as a function of equilibrium volume based on the present first-principles results by PBEsol. Both B_0V_0 and $f_{s0}r_0^2$ show that Y, Zr, and especially Hf increase the M—O bonding energy with respect to the Al—O case, whereas the La—O bonding energy is weaker. However, the predicted Cr—O and especially Ti—O bonding energies have large differences from B_0V_0 and $f_{s0}r_0^2$. For example, it shows that a faster-growing Al_2O_3 scale results from Ti addition based on $f_{s0}r_0^2$; whereas, a slower-growing Al_2O_3 scale results from Ti addition based on B_0V_0. Fig. 2b shows the measured T_m values and the $-\Delta H_{298}$ values for the oxides of interest (estimated by the SSUB5 database) [25]. Note that (i) the gas constant R in Eq. (2) is ignored since it is a constant and (ii) the unit of ΔH_{298} is energy per mole metal atoms to normalize the number of M—O bonds in oxygen-rich MO_2 and M_2O_3. Similar to the conclusions from Fig. 2a, Y, Zr, and especially Hf have unambiguously stronger M—O bonding energy than that of Al—O in terms of T_m and $-\Delta H_{298}$. In addition, Ti—O has a weaker bonding energy than Al—O. However, Cr—O has a stronger bonding energy from T_m whereas a weaker bonding energy from $-\Delta H_{298}$ with respect to the Al—O case.

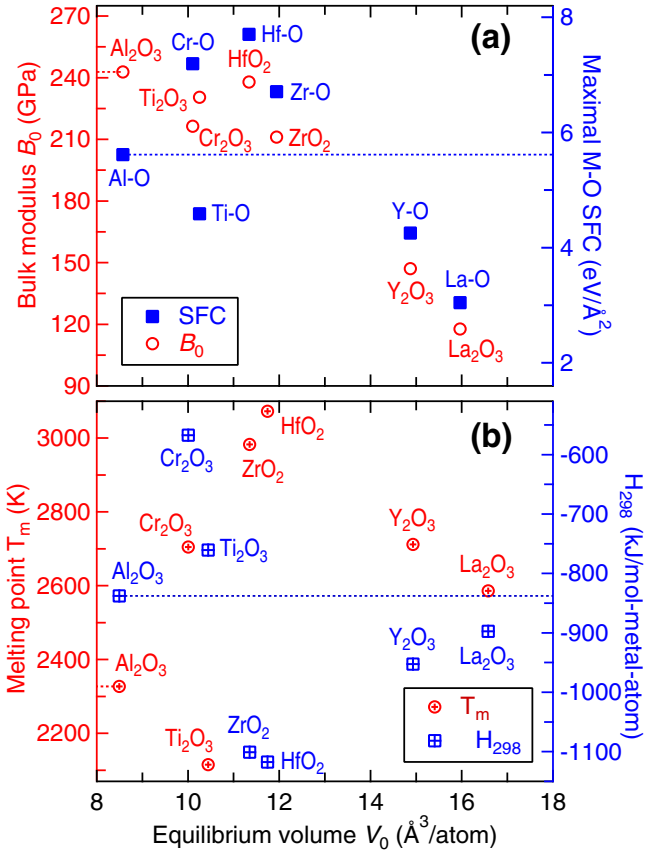

Fig. 2. Metal-oxygen bonding energies related to the stretching force constant ($f_{s0}r_0^2$) and bulk modulus (B_0V_0) predicted by PBEsol in the present work (a), and the melting point (T_m) and enthalpy of formation at 298 K ($-\Delta H_{298}$) from experiments [25] (b); see the models in Eqs. (2) and (3).

Table 1
Summary of alumina (α-Al_2O_3) scale from the slow- to fast-growing rate affected by alloying elements (REs and Cr) characterized by the metal-oxygen bonding energy, which is related to the properties of stretching force constant ($f_{s0}r_0^2$), bulk modulus (B_0V_0), melting point (T_m), and enthalpy of formation at 298 K ($-\Delta H_{298}$) of oxides; see the models in Eqs. (2) and (3).

Properties	Slow-growing scale by	Fast-growing scale by	Details in
$f_{s0}r_0^2$	Hf → Cr, Zr → Y→	Ti, La	Fig. 2a (this work)
B_0V_0	Hf → Zr → Ti → Y, Cr→	La	Fig. 2a (this work)
T_m	Hf → Zr → Cr, Y → La→	Ti	Fig. 2b (expt.) [25]
$-\Delta H_{298}$	Hf, Zr → Y → La→	Ti → Cr	Fig. 2b (expt.) [25]

Table 1 summarizes the M—O bonding energies presented in Fig. 2. It shows that all models in Eqs. (2) and (3) indicate Hf—O has the highest bonding energy, making Hf the best reactive element in retarding the growth of Al_2O_3 scale. The other beneficial REs for the slow-growing Al_2O_3 scale are Zr and Y. However, the discrepancies are for Cr, Ti and La, which may promote or retard the Al_2O_3-scale growth rate. Alloying element Cr can dissolve in Al_2O_3 [1], increasing Cr—O SFCs (see Fig. 1a), and in turn, a stronger Cr—O bonding energy. It is therefore concluded that Cr should retard the growth of Al_2O_3 scale. Reactive element La (as well as Y) has quite a large ionic size, such as r_0 = 2.35 Å for La—O versus r_0 = 1.86 Å for Al-O; see Supplementary Table S1. Any decrease of La—O bond length when La locates on the grain-boundary of Al_2O_3 will increase greatly the La—O bonding strength (see Fig. 1a). This suggests that La could retard the growth of Al_2O_3 scale. For the smaller ionic size of Ti, we conclude that Ti promotes the growth of Al_2O_3 scale to some extent.

It should be mentioned that over-doping of REs will promote the formation RE-containing oxides and hence result in an accelerated oxidation process. An optimal amount of RE addition needs to be determined by using such as thermodynamic modeling, see the approach to guide Hf-doping in the Al_2O_3-forming NiCrAl alloys [9]. Note also that the RE—O bonding strength/energy cannot explain the observation that Hf only suppressed Al diffusion during polycrystalline alumina wafers exposed to oxygen potential [26], albeit this experiment is not fully consistent with the observations in alumina scales [7].

In summary, the determination of local bonding energy between two atoms of interest has been proposed in terms of the stretching force constants (SFC), see Eq. (3). Based on force constants from first-principles phonon calculations of oxides (Al_2O_3, Cr_2O_3, Ti_2O_3, ZrO_2, HfO_2, Y_2O_3, and La_2O_3), Al_3X compounds, and the dilute M-containing $Al_{47}MO_{72}$ (M = Cr, Ti, Zr, Hf, Y, and La), we quantify the M-O bonding energies using the present SFC model. Together with the M—O bonding energies estimated from the global properties of oxides, i.e., bulk modulus, melting point, and enthalpy of formation; see the models in Eq. (2), we conclude that the slow-growing alumina scale tuned by reactive elements (REs) can be explained by the strong RE—O bonding energy. It is found that Hf is the best RE to retard the growth of alumina scale, followed by Zr, Y, and La. Our predictions are in good agreement with experimental observations [1,5,6,8,9], indicating the capability of the present SFC model to understand the slower-growing alumina scale affected by reactive elements.

Acknowledgments

This work was funded by the U.S. Department of Energy through Grant DE-FE0024056. First-principles calculations were carried out partially on the LION clusters supported by the Materials Simulation Center and the Research Computing and Cyber infrastructure unit at the Pennsylvania State University, partially on the resources of NERSC supported by the Office of Science of the U.S. DOE under Contract No. DE-AC02-05CH11231, and partially on the resources of XSEDE supported by National Science Foundation with Grant ACI-1053575.

Appendix A. Supplementary data

Supplementary data to this article can be found online at https://doi.org/10.1016/j.scriptamat.2018.03.002.

References

[1] P.Y. Hou, J. Am. Ceram. Soc. 86 (2003) 660–668.
[2] B.A. Pint, M. Treska, L.W. Hobbs, Oxid. Met. 47 (1997) 1–20.
[3] N.P. Padture, Science 296 (2002) 280–284.
[4] B.W. Veal, A.P. Paulikas, P.Y. Hou, Nat. Mater. 5 (2006) 349–351.
[5] A.H. Heuer, T. Nakagawa, M.Z. Azar, D.B. Hovis, J.L. Smialek, B. Gleeson, N.D.M. Hine, H. Guhl, H.-S. Lee, P. Tangney, W.M.C. Foulkes, M.W. Finnis, Acta Mater. 61 (2013) 6670–6683.
[6] Y. Chen, R.C. Reed, E.A. Marquis, Oxid. Met. 82 (2014) 457–467.
[7] D. Naumenko, B.A. Pint, W.J. Quadakkers, Oxid. Met. 86 (2016) 1–43.
[8] D.E. Kim, S.-L. Shang, Z.Q. Li, B. Gleeson, Z.-K. Liu, Oxid. Met. (2018) (Submitted).
[9] T. Gheno, B.-C. Zhou, A. Ross, X. Liu, G. Lindwall, Z.-K. Liu, B. Gleeson, Oxid. Met. 87 (2017) 297–310.
[10] J. Cho, H.M. Chan, M.P. Harmer, J.M. Rickman, J. Am. Ceram. Soc. 81 (2005) 3001–3004.
[11] A.H. Heuer, D.B. Hovis, J.L. Smialek, B. Gleeson, J. Am. Ceram. Soc. 94 (2011) s146–s153.
[12] S.L. Shang, L.G. Hector Jr., Y. Wang, H. Zhang, Z.K. Liu, J. Phys. Condens. Matter 21 (2009) 246001.
[13] S. Shang, Y. Wang, P. Guan, W.Y. Wang, H. Fang, T. Anderson, Z.-K. Liu, J. Mater. Chem. A 3 (2015) 8002–8014.
[14] J.Z. Liu, G. Ghosh, A. van de Walle, M. Asta, Phys. Rev. B 75 (2007) 104117.
[15] G. Kresse, J. Furthmüller, Phys. Rev. B 54 (1996) 11169–11186.
[16] G. Kresse, D. Joubert, Phys. Rev. B 59 (1999) 1758–1775.
[17] J.P. Perdew, A. Ruzsinszky, G.I. Csonka, O.A. Vydrov, G.E. Scuseria, L.A. Constantin, X. Zhou, K. Burke, Phys. Rev. Lett. 100 (2008) 136406.
[18] S.P. Ong, W.D. Richards, A. Jain, G. Hautier, M. Kocher, S. Cholia, D. Gunter, V.L. Chevrier, K.A. Persson, G. Ceder, Comput. Mater. Sci. 68 (2013) 314–319.
[19] A. Jain, S.P. Ong, G. Hautier, W. Chen, W.D. Richards, S. Dacek, S. Cholia, D. Gunter, D. Skinner, G. Ceder, K.A. Persson, APL Mater. 1 (2013) 11002.
[20] S.-L. Shang, Y. Wang, D. Kim, Z.-K. Liu, Comput. Mater. Sci. 47 (2010) 1040–1048.
[21] Y. Wang, S.-L. Shang, H. Fang, Z.-K. Liu, L.-Q. Chen, NPJ Comput. Mater. 2 (2016) 16006.
[22] Q. Wu, H.M. Chan, J.M. Rickman, M.P. Harmer, J. Am. Ceram. Soc. 98 (2015) 3346–3351.
[23] S.-L. Shang, B.-C. Zhou, W.Y. Wang, A.J. Ross, X.L. Liu, Y.-J. Hu, H.-Z. Fang, Y. Wang, Z.-K. Liu, Acta Mater. 109 (2016) 128–141.
[24] M.F. Ashby, Proc. R. Soc. A Math. Phys. Eng. Sci. 454 (1998) 1301–1321.
[25] Lehrstuhl fuer Theoretische Huettenkunde (Ed.), Scientific Group Thermodata Europe (SGTE), Landolt-Boernstein New Ser. Gr. IV, Springer, Verlag Berlin Heidelberg, 1999.
[26] T. Matsudaira, M. Wada, T. Saitoh, S. Kitaoka, Acta Mater. 59 (2011) 5440–5450.